ELSEVIER

Journal of Materials Processing Technology 130–131 (2002) 31–41

Journal of Materials Processing Technology

www.elsevier.com/locate/jmatprotec

Formability analysis of extra-deep drawing steel

D. Ravi Kumar

Department of Mechanical Engineering, Indian Institute of Technology Delhi, New Delhi 110 016, India

Abstract

In the present work, formability of five sheets of aluminum-killed extra-deep drawing (EDD) low carbon steel sheets (with a wide variation in thickness) has been characterized. Forming limit diagrams (FLDs) have been determined experimentally by conducting punch-stretching experiments using suitably designed and fabricated tools. Formability, observed from FLDs, has been correlated with microstructure, mechanical properties and formability parameters like strain hardening coefficient (n) and normal anisotropy ($\bar{r}$). The strain distribution in the material during punch-stretching under different states of strain has been studied. From the experimental results, it has been found that four of the five sheets have a favorable grain size and mechanical properties to meet the requirements of good formability. The suitability of these sheets for critical deep-drawing applications has been examined in terms of the level and range of critical strains in the FLD. These results correlated well with formability parameters. Earing tendency during drawing is expected to be high for one sheet due to its high planar anisotropy. The level of the FLD increased significantly with the sheet thickness. The effect of n and $\bar{r}$ on the strain distribution characteristics has been analyzed.

Keywords: Forming limit diagram; Extra-deep drawing steel; Strain hardening coefficient; Normal anisotropy; Strain distribution

1. Introduction

Complex stampings are required for today's automotive and various other industries. Such stampings are now developed with the aid of data obtained from laboratory experiments that enables the press formability of sheet metals to be reliably predicted. Therefore, an understanding of the formability of sheet metals is essential for the successful production of quality stampings. In forming a sheet into a specific shape, since the design variables are fixed, the process variables have the greatest influence on the overall formability and are usually assessed during die tryout. However, in shop floor manufacture, process variables are optimized to yield maximum production rates at minimum cost and therefore, maximum exploitation of material ductility is greatly dependent upon the material properties.

However, due to the complex interaction of large number of variables, which affect formability of sheet metals, there is no single parameter, which can comprehensively describe the forming characteristics of a material under various conditions in actual press working. Although the quest for such a parameter has proved to be elusive till date, efforts in that direction remain unremitting.

2. Scope and objectives of the present study

Extra-deep drawing (EDD) steels are the most widely used steel material today for automotive applications involving simple to complex stampings which require very high formability, mainly stretchability and drawability. Exterior components such as starter end covers, petrol tanks, etc., are made up of deep-drawing grade steels. Automobile industry apart, the low carbon steel sheets are used extensively in enameling applications such as baths, sink units, kitchen ware, cooker and refrigerator panels, etc.

In the present work, formability of five heats of indigenously produced aluminum-killed EDD low carbon steel sheets has been characterized in terms of their microstructure, mechanical properties and forming limit diagram (FLD). Sheets with a wide variation in thickness (0.8–2.0 mm) and the normal anisotropy parameter $\bar{r}$ value (1.0–1.6) were chosen for the present study. The principal aim has been to obtain in a quantitative manner the effect of variation in $\bar{r}$ and the corresponding texture level upon press formability. The sheets had thickness of 0.8, 1.0, 1.25, 1.6, and 2.0 mm (and will be referred to as heats A, B, C, D and E, respectively, hereafter). All the sheets were received in cold rolled and annealed condition.

0924-0136/02/$ – see front matter
PII: S0924-0136(02)00789-6

3. Experimental work

The various experimental methods an techniques followed in the present investigations are described in this section.

3.1. Chemical composition and grain size

The chemical composition of the materials (in wt.%) used in the present investigations was analyzed by an emission spectrometer (ARL 3460 metals analyzer). The nitrogen content (in ppm) was estimated in the EDD steel samples using a Leco gas analyzer. Samples for optical microscopy, prepared following procedures of standard metallographic practice, were observed under the optical microscope with a view to obtaining a correlation between microstructural aspects and mechanical behavior. The two-dimensional grain size was measured using the average linear intercept method at different magnifications.

3.2. Tensile properties and hardness

Tensile tests were carried out using specimens machined as per ASTM standard E8M specification. The specimens were tested along the three directions, with the tensile axis being parallel (0°), diagonal(45°), and perpendicular (90°) to the rolling direction of the sheet, on a 400 kN capacity Schenck closed-loop servo-hydraulic testing machine. The standard tensile properties namely, 0.2% yield stress (YS), ultimate tensile stress (UTS), uniform elongation (e_u), total elongation (e_f), strain hardening exponent (n) and strength coefficient (K) were determined from the load–elongation data obtained from these tests. A constant cross head speed of 0.5 mm min^{-1} (corresponding to an initial strain rate of 2.78×10^{-4} s^{-1}) was employed in all cases. Three samples were tested in each of the three directions and average values were reported to account for the scatter.

Strain rate sensitivity index, m, was calculated from the results of strain rate jump tests carried out on tensile specimens. The strain rate was suddenly increased during the uniform plastic deformation and in such a strain rate change test, m is defined [1] as

$$m = \frac{\ln(\sigma_2/\sigma_1)}{\ln(\varepsilon_2/\varepsilon_1)} = \frac{\ln(P_2/P_1)}{\ln(V_2/V_1)} \quad (1)$$

where σ_1 and σ_2 are flow stress values at strain rates $\dot{\varepsilon}_1$ and $\dot{\varepsilon}_2$, respectively. P_1 and P_2 are loads corresponding to cross head speeds of V_1 and V_2, respectively.

The hardness value (in Rockwell scale B) of the five heat of EDD steels in the as-received conditions were measured using 100 kgf load, 1/16 in. diameter steel ball with a load application for 20 s.

3.3. Formability parameters

The strain hardening exponent n, the plastic strain ratio r (the ratio of true width strain to true thickness strain) and the planar anisotropy Δr are the conventional indicators of formability of sheet metals. The stain hardening exponent n was determined from the regression of the load–elongation data obtained from the tensile tests, using the Hollomon equation, $\sigma = K\varepsilon^n$. The r value was evaluated following the procedure of Liu and Johnson [2], the specimens were deformed incrementally at equally spaced intervals and the major and minor strains were measured in the gauge length (marked in the central portion of the specimen). The r value was then evaluated from the slope (S) of the plot of ε_2 versus ε_1 using the relation $r = -S/(1 + S)$. This procedure gives a strain independent value for r and also normalizes any experimental scatter. The r value was evaluated in the three directions as in tensile tests specified above. The normal anisotropy, $\bar{r}$ and the planar anisotropy Δr were calculated using the standard formulae [3]:

$$\bar{r} = \tfrac{1}{4}(r_0 + 2r_{45} + r_{90}), \qquad \Delta r = \tfrac{1}{2}(r_0 - 2r_{45} + r_{90}) \quad (2)$$

where the subscripts indicate the orientation of the specimen axis with respect to rolling direction.

3.4. Forming limit diagrams (FLDs)

The FLD was evaluated following Hecker's simplified technique [4]. In this method, the experimental procedure mainly involves three stages—grid marking the sheet specimens, punch-stretching the grid-marked samples to failure or onset of localized necking and measurement of strains.

Grid marking on the sheet samples of Al-killed EDD steel was done using a non-contacting grid of 5 mm diameter circles. The grid pattern was etched on the samples using an electro-chemical etching equipment. Punch-stretching experiments were carried out on a 1000 kN (100 t) capacity double-action hydraulic press. Different punch-die assemblies were designed and fabricated depending on the thickness of the sheets. A typical punch-die assembly used in the experiments is shown in Fig. 1. The sheet samples were subjected to different states of stain, i.e. the tension–tension zone, plane strain and the tension-compression zone by varying the width of the sample [5,6]. The length of the blank was 200 mm and width was varied between 200 and 25 mm in steps of 25 mm. For each blank width, at least four to five specimens were tested to get maximum number of data points. To obtain the maximum values in the magnitude of the negative minor strain, uniaxial tension tests were also done using grid-marked of localized specimens. The blanks were stretched to failure and the experiments was stopped at the time of onset of localized necking in some cases and continued till failure in other cases.

The circles on the sheet samples became ellipses after deformation, falling into safe, necked and failed zones. The major and minor diameters of the ellipses using a flexible scale, were plotted against each other. The FLD was then drawn clearly demarcating the safe limiting strains from the unsafe zone containing the necked and fractures ellipses. The accuracy of the FLD lies well within a band of ±2% in the engineering strain values.

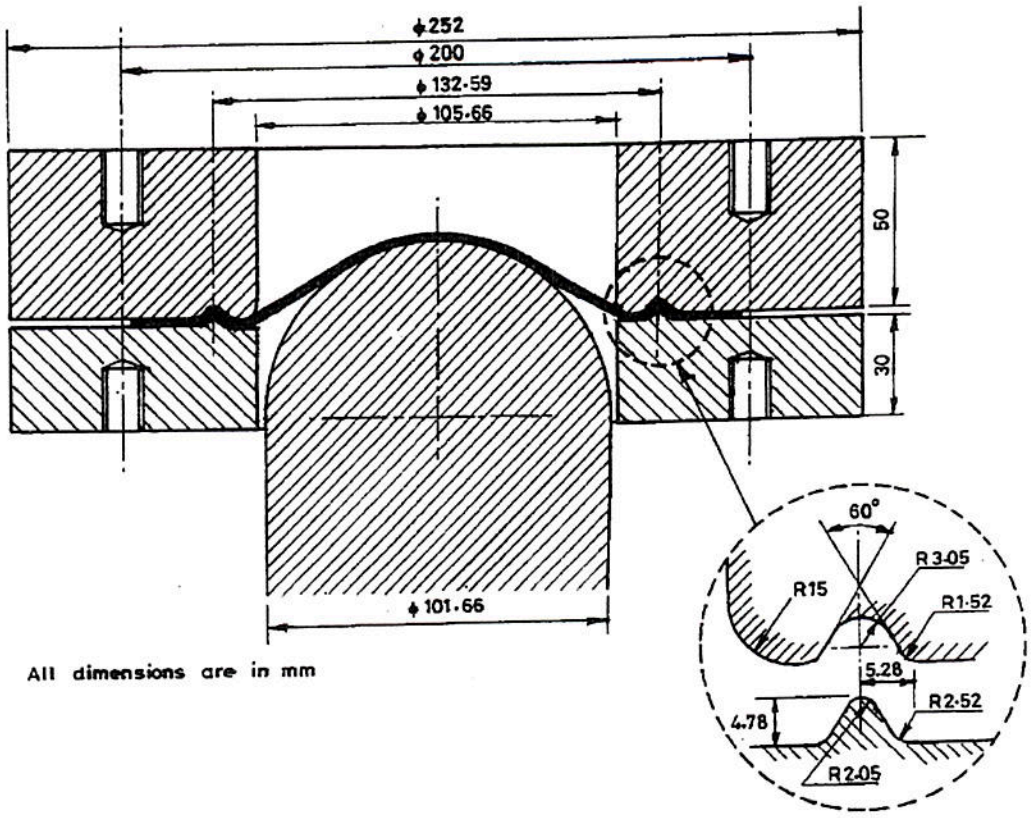

Fig. 1. Punch-die assembly used for punch-stretching experiments of EDD steel sheets (for heats A, B and C).

3.5. Strain distribution profiles

To represent the strain distribution in the material during punch-stretching under different states of strain, samples of each blank width which were deformed to crack initiation or to the onset of severe localized necking were selected. The major and minor strains were measured for all the ellipses along the longitudinal direction of the sample and lying at the center of the blank, which represent the radial and tangential strains in the samples at those locations. The ellipse which lies exactly under the punch, usually undergoes minimum deformation and it lies at the center of the longitudinal meridian of the deformed sample. The center of this ellipse is referred to as the pole. The radial and tangential strains were plotted as a function of their distance from the pole. Sometimes, it is preferred to consider thickness strain instead of radial and tangential strains. Hence thickness strain distributions were also evaluated by calculating thickness strain from the other two principal strains.

4. Results and discussion

4.1. Chemical composition

The chemical compositions of the five heats of the EDD aluminum-killed steel sheets are given in Table 1. The amount of carbon in all the five heats was in the range 0.06–0.08%, which is higher than the desired carbon level for good drawability. Higher carbon content leads to a decrease in the formability parameter, $\bar{r}$. This is attributed to an increase in the amount of cementite and a decrease in grain size. High $\bar{r}$ values (>1.6) have been observed in case of EDD steel sheets containing carbon less then 0.05% [7]. In the present study, since the difference in the carbon content among the five heats is insignificant, any variation in their formability cannot arise from carbon levels. Mizui and Okamoto [8] studied the effect of Mn content (in the range 0.02–0.14%) on deep drawability of continuous annealed Al-killed sheet steels. They concluded that the r

Table 1
Chemical composition of five heats of Al-killed EDD steel sheets (in wt.%)

Element	Heat A (0.8 mm)	Heat B (1.0 mm)	Heat C (1.25 mm)	Heat D (1.6 mm)	Heat E (2.0 mm)
Carbon	0.077	0.065	0.078	0.068	0.068
Manganese	0.340	0.342	0.370	0.312	0.340
Silicon	0.020	0.035	0.013	0.017	0.022
Phosphorous	0.012	0.019	0.021	0.014	0.015
Sulfur	0.010	0.035	0.025	0.010	0.016
Aluminum	0.098	0.013	0.053	0.064	0.066
Nitrogen (ppm)	112	73	32	77	112
Iron	Balance	Balance	Balance	Balance	Balance

value in the rolling direction exhibited a maximum value at a medium Mn content which increases with increase in the coiling temperature. They attributed this to the changes in the distribution of MnS inclusion and the precipition of Al/N. Dasarathy and Hudd [9] indicated that the presence of aluminum up to 0.08% had no adverse effect on the mechanical properties. Only in heat A, the Al content exceeded this value. More importantly, it is the ratio of aluminum to nitrogen contents which affect the formability significantly. The desired ratio of aluminum to nitrogen is around 10 [10]. The presence of soluble aluminum and nitrogen help in precipitation of aluminum nitride which is beneficial for the development of the desired {1 1 1} texture component and thereby achieving a high $\bar{r}$ value. Singh [11] indicated that the best $\bar{r}$ value can be obtained with 0.04–0.07% Al (total) and 0.0065–0.0095% N. Only heat D falls in this range and hence a favorable texture and a high $\bar{r}$ value would be expected for this heat.

4.2. Grain size

The microstructures of the five heats in the as-received condition were studied using optical microscopy and the values of average grain size, determined by the linear intercept method, are 11, 23, 19, 25 and 29 μm for the five heats, respectively. These values are accurate to within ±2 μm. The grain sizes of all the heats except heat A lie in the range of ASTM nos. 7–8, which is typical of drawing quality steels. The investigations of Wilson and Acselrad [12] on the effect of grain size on the behavior of low carbon steel showed that the favorable grain size for good formability is in the range of 20–45 μm. It has been shown that both strain hardening exponent, n and average plastic strain ratio, $\bar{r}$ increased with increase in grain size. The $\bar{r}$ value and grain size of aluminum stabilized steels concurrently increased by annealing at high temperature up to the point of transformation. The effect of annealing temperature and hence grain size on the $\bar{r}$ value of a titanium bearing steel has been shown to be significant. Except heat A, all other heats have a grain size in the desired range. Also, the limit of thickness strain was observed to depend on the t_0/d_0 ratio where t_0 is the thickness of the sheet and d_0 is the average grain diameter and Wilson et al. [13] found that it increases with increase in t_0/d_0 ratio, with highest thickness strain reported for a t_0/d_0 ratio in the range 60–75. This ratio lies in the range for heats A, C, D and E and it is relatively low for heat B.

4.3. Mechanical properties

The hardness values (in Rockwell scale B) of the five heats in the as-received condition, measured using 100 kgf load, 1/16 in. diameter steel ball with a load application for 20 s are given in Table 2. The value lie in the range of 41–49 HR_B, typical of deep-drawing steels.

The room temperature mechanical properties of the five heats, determined by tensile testing with the specimen axis oriented at 0°, 45°, and 90° to the rolling direction, are reported in Table 2. In most cases, the UTS values were higher at 45° to the rolling direction than in the direction

Table 2
Mechanical properties of EDD steel[a]

Heat	Orientation w.r.t. RD (°)	YS (MPa)	UTS (MPa)	Uniform elongation (%)	Total elongation (%)	Strain rate sensitivity index, m	Hardness (HR_B)
Heat A	0	197.5	315.0	31.8	39.4		
	45	194.5	328.5	28.5	37.9		
	90	195.0	315.0	31.3	39.5		
Average		195.4	321.8	30.0	38.7	0.012	41
Heat B	0	248.7	329.6	24.8	35.0		
	45	252.6	328.3	22.0	29.9		
	90	226.1	314.1	20.8	30.5		
Average		245.0	325.1	22.4	31.3	0.009	49
Heat C	0	208.9	292.9	29.2	44.2		
	45	232.8	314.0	24.5	36.3		
	90	220.8	292.7	25.3	38.9		
Average		223.8	303.4	25.9	38.9	0.010	46
Heat D	0	182.2	291.7	30.4	46.3		
	45	193.7	307.5	31.3	44.1		
	90	186.0	291.0	30.3	46		
Average		188.9	299.4	30.8	45.2	0.014	45
Heat E	0	199.2	274.2	28.1	43.4		
	45	202.4	279.2	28.3	39.7		
	90	207.2	274.6	28.8	43.9		
Average		202.8	276.8	28.4	41.7	0.012	44

[a] Average, $X = (X_0 + 2X_{45} + X_{90})/4$.

Table 3
Formability parameters of Al-killed EDD steel sheets[a]

	Heat A	Heat B	Heat C	Heat D	Heat E
n	0.25	0.17	0.21	0.25	0.22
r_0	1.32	1.03	1.65	1.63	1.48
r_{45}	0.96	0.85	1.26	1.23	1.14
r_{90}	1.52	1.31	2.06	2.25	1.74
$\bar{r}$	1.19	1.01	1.56	1.58	1.37
$n\bar{r}$	0.29	0.18	0.29	0.37	0.28
Δr	0.46	0.32	0.60	1.02	0.47

[a] $\bar{r} = (r_0 + 2r_{45} + r_{90})/4$, $\Delta r = (r_0 - 2r_{45} + r_{90})/2$.

Table 4
Strain hardening exponent (n) of EDD steel sheets from different methods

Heat	From regression	From $n = \varepsilon_u$	From Eq. (3)	From Eq. (4)
Heat A	0.25	0.26	0.16	0.26
Heat B	0.17	0.20	0.16	0.30
Heat C	0.21	0.23	0.16	0.28
Heat D	0.25	0.27	0.17	0.31
Heat E	0.22	0.25	0.16	0.31

parallel or perpendicular to the rolling direction while the elongation to fracture was greater along the rolling direction than along directions perpendicular or diagonal to the same. Heat B exhibited higher strength values and lower ductility. Its strain hardening exponent value is also low indicating its inferior stretchability.

The strain rate sensitivity index (m) determined by strain rate jump tests [11], was found to be very similar for all the three directions, i.e. 0°, 45°, and 90° to the rolling direction and the m values are also reported in Table 2, which are seen to be very small but positive. This is consistent with the fact that most of the common metals like low carbon steel have very low sensitivity to the strain rate at room temperature.

4.4. Formability parameters

The conventional indicators of formability, viz., the strain hardening exponent n (obtained from regression of the Hollomon equation $\sigma = K\varepsilon^n$), average plastic strain ratio, or normal anisotropy $\bar{r}$ (determined using Liu and Johnson's technique), the product $n\bar{r}$ and planar anisotropy Δr, for all the heats are summarized in Table 3. The strain hardening exponent n is high (in the range of 0.20–0.25) for all heats except heat B indicating their excellent stretchability. Among the five heats, heat B is expected to possess low formability as in evident from its low n and $\bar{r}$ values.

As given in Table 3, the product $n\bar{r}$ which is indicative of overall press performance factor, is high for heats A, C and D. As expected, heat B has the lowest value. However, this factor has no physical significance and it is only a numerical index used as a rough measure of formability [14]. The planar anisotropy value, which gives an idea about the type of earing that occurs during drawing of sheet metals, is rather high in all cases, with heat D having the highest value, making it most susceptible to earing problem among the five heats studied. It is consistent with the fact that a sheet with a high $\bar{r}$ value generally possess a high Δr value also. It is to be noted that the ideal situation of a high $\bar{r}$ and a low Δr is difficult to achieve under normal processing conditions.

4.4.1. Strain hardening exponent

It has already been emphasized that the stretchability of sheet metals is strongly influenced by the value of strain hardening exponent. Table 3 gives the n values of five heats of EDD steel sheets determined by various methods. From the table it can be seen that the values obtained from true uniform strain in tensile tests ($n = \varepsilon_u$) agreed well with the values obtained from regression of the Hollomon equation $\sigma = K\varepsilon^n$ (also reported in Table 4). But, the values obtained by equating n to the true uniform strain, calculated using an empirical relationship [15] for low carbon mild steels are much lower than generally expected for low carbon steels. This empirical equation is reproduced below.

$$\varepsilon_u = 0.28 - 0.2[\mathrm{C}] - 0.25[\mathrm{Mn}] - 0.44[\mathrm{Si}] - 0.39[\mathrm{Sn}] - 1.2[\mathrm{N}] \quad (3)$$

The values obtained from the above equation are almost equal for all heats. It could be due to the similar composition of all heats and the fact that other factors like grain size, heat treatment, on which n greatly depends, are not taken into account. Clearly this empirical equation has very limited applicability.

The relationship between n and grain size, d is as follows [13]:

$$n = \frac{5}{10 + d^{-1/2}} \quad (4)$$

The n values obtained based on the above equation are higher than those obtained from other three methods. However, only the values obtained from the regression analysis are used in all further discussions.

4.4.2. Average plastic strain ratio

Table 5 gives the values of average plastic strain ratio or normal anisotropy $\bar{r}$ obtained using three different methods. It can be observed that the $\bar{r}$ value is higher for heats C and D indicating their good drawability. Heats A and B have low $\bar{r}$

Table 5
Normal anisotropy ($\bar{r}$) of EDD steel sheets from different methods

Heat	From ASTM E517 method	From Liu and Johnson method	From Module-r tester
Heat A	0.95	1.19	1.12
Heat B	1.18	1.01	0.98
Heat C	1.42	1.56	1.55
Heat D	1.55	1.58	1.63
Heat E	1.33	1.37	1.40

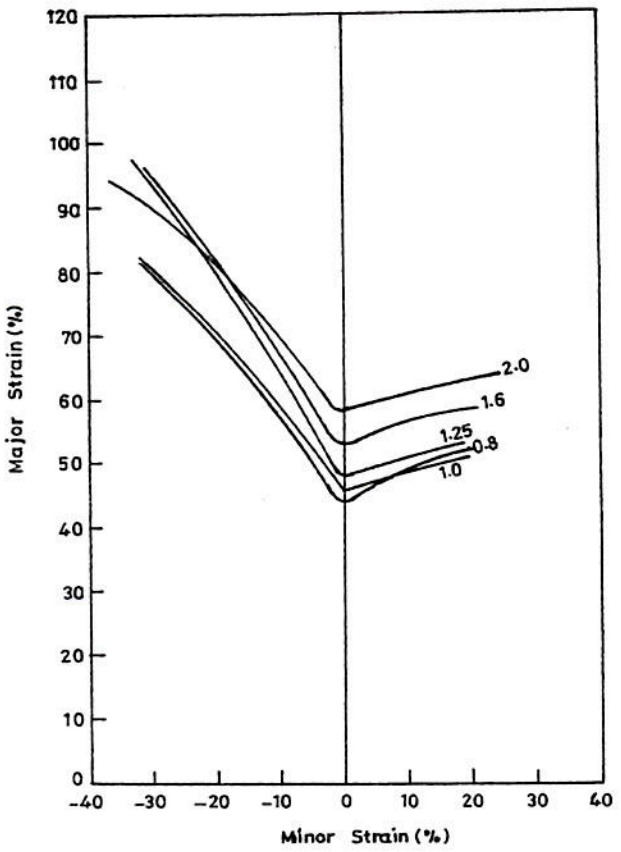

Fig. 2. A comparison of the FLDs of five heats of the EDD steel.

value indicating their inferior drawability while that of heat E is moderate. The $\bar{r}$ values determined using Liu and Johnson's technique agreed closely with those determined using Module-$\bar{r}$ tester. But the $\bar{r}$ values obtained from ASTM E517 method are lower compared with the other two methods in all cases except heat B. But the advantage of Liu and Johnson's method over the ASTM method is that it is strain independent and also normalizes any experimental scatter. Hence these values are viewed as more correct and indicative of true drawability.

4.5. Forming limit diagrams (FLDs)

FLDs, evaluated experimentally for the Al-killed EDD steel sheets following Hecker's method, are shown in Fig. 2.

The FLDs of all the five heats are reasonably consistent with expectations based on the uniaxial tensile properties. The effect of sheet thickness on the level of the FLD is clearly seen, particularly at the plane strain condition ($e_2 = 0$). The level of the FLD increased with increase in sheet thickness. In the biaxial tension region, the limit strains of heat A are higher than those of heat B despite its slightly lower thickness. This can be attributed to its much higher n values (0.25) when compared to heat B ($n = 0.17$). The slopes of the FLDs and the limit strain of the left-hand side are consistent with the $\bar{r}$ values. Heat D (1.6 mm) and heat C (1.25 mm) exhibited very high limit strain values. All heats excepts heat B have good stretchability while only heats C and D have excellent drawability.

From the above discussion, it can be seen that FLDs are consistent with the mechanical properties and microstructural features to a large extent. But some features are difficult to explain. For example, heat A showed better stretchability than heat B despite of its lower thickness and higher oxygen content, which are supposed to lower the formability. The $\bar{r}$ value of heat C is higher than that of heat A despite the latter's very high Al/N ratio. However, heat C has a much coarser grain size than heat A which favors a high $\bar{r}$ value. Any minor discrepancy in the relative overall formability of five heats could be due to the complex interaction of large number of variables and hence it is clearly impossible to single out any parameter to completely explain formability limits of a heat with respect to other heats.

4.6. Strain distribution profiles

The strain distribution profiles were plotted for all the blank widths by measuring the major and the minor strains along the longitudinal direction of the specimens of all the five heats. Due to constraint on the length of the paper, strain distribution is shown only for heat D (Fig. 3(a)–(h)). The following features have been observed from the strain distribution profiles:

1. Two distinct peaks were observed in major strain for all the blank widths and these peaks were located symmetrically on either side of the pole (the center for the ellipse that is lying exactly above the punch is referred to as pole and it is also the region which has undergone minimum amount of deformation).
2. In case of minor strain, a similar trend was observed for blank widths 200, 175 and 150 mm which fall in biaxial stretching mode. For blank widths 125 and 100 mm, the strain is almost zero indicating plane strain condition. Below a blank width of 150 mm the minor strain is almost zero indicating plane strain condition (the clamping bead diameter being 132 mm) due to decreased degree of gripping efficacy. So the minor strain progressively goes down. When the blank width was decreased to 100 mm, minor strain become negative due to lateral drawing-in and with further decrease in blank width, the minor strain developed two peaks with negative values.
3. The asymmetry observed in the magnitude of strain peaks on either side of the pole could be due to the fact when fracture initiated of strain peaks on either side of the pole, the load ceased to act on the other side which was in either safe or necked zone and hence the deformation did not proceed further in that region. In addition, the difficulty in achieving perfectly symmetrical loading in real/actual press-working practice and the additional factor of local inhomogeneities being

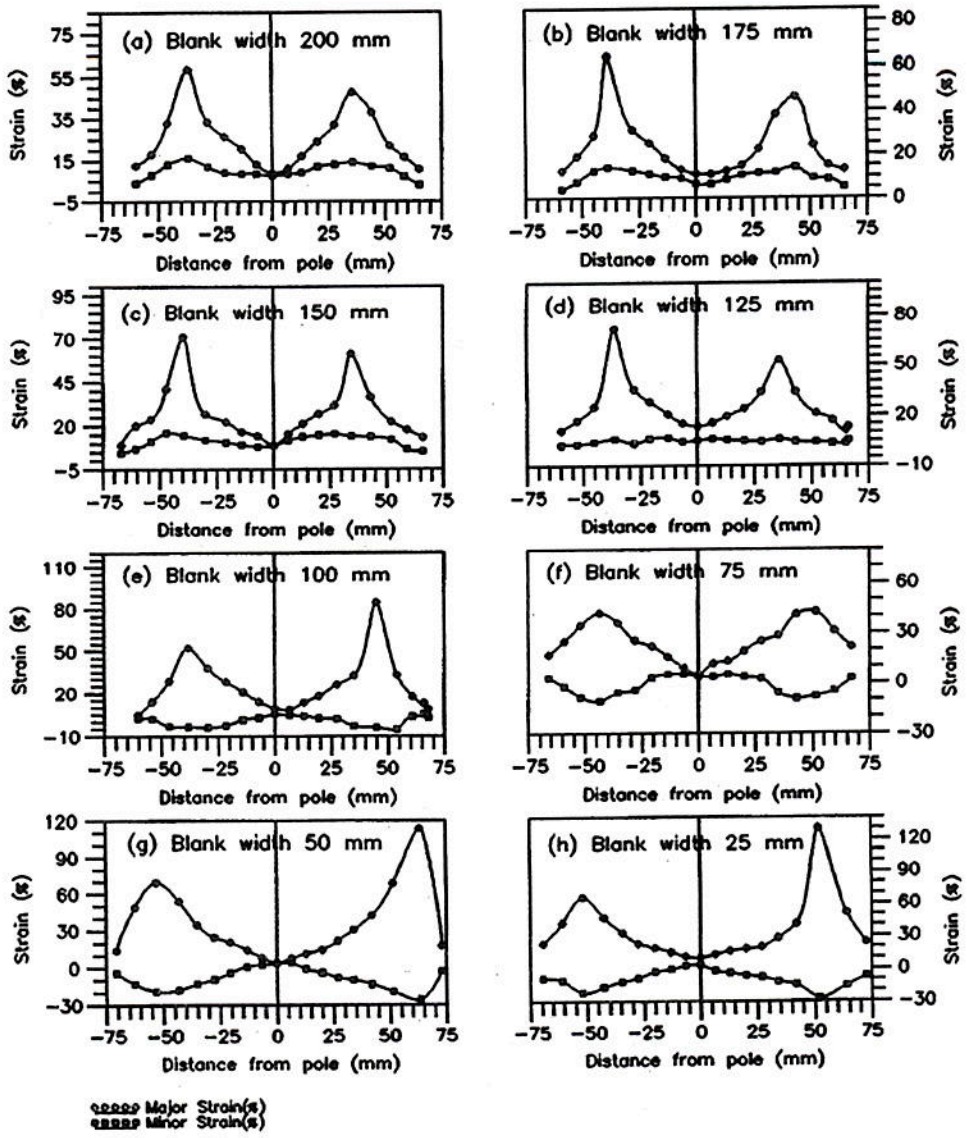

Fig. 3. Longitudinal strain distribution profiles in the punch-stretched blanks of EDD steel (heat D) for various blank widths.

present in the sheet metal could also have played a minor role.

4. As the blank width decreased, the separation between the two peaks increased progressively because of the increased lateral drawing-in of the sheet metal, i.e. the location of the strain peaks moved towards the die throat.
5. The variation of the average distance from pole to peak with blank width is similar for all the heats. It increased with decreasing blank width and follows from point 4 mentioned above. A similar observation was made earlier in case of materials with $\bar{r}$ value greater than unity [16].
6. In most cases, the strain ratio at failure approached plane strain which is generally the case for drawing steels ($r > 1$) [16].

4.6.1. Thickness strain distribution

It is sometimes preferred to know the variation of strain in thickness direction during deformation because the failure in sheet metal forming usually occurs by thinning or localized necking. Hence thickness strain was calculated from the values of principal surface strains using the relation $\varepsilon_1 + \varepsilon_2 + \varepsilon_3 = 0$. The thickness strain for three blank widths (200, 100 and 25 mm which represent three different stress states, i.e. biaxial tension, plane strain condition and tension-compression) is plotted against distance from the pole. These thickness strain distribution profiles are shown in Fig. 4(a)–(c) for heats, A, B, C, D and E, respectively. As can be seen from these figures, the peak thickness strain shifted to towards the die throat as the blank width decreased. Also it can be noted that the limit thickness strains are higher in biaxial stretching (200 mm) and

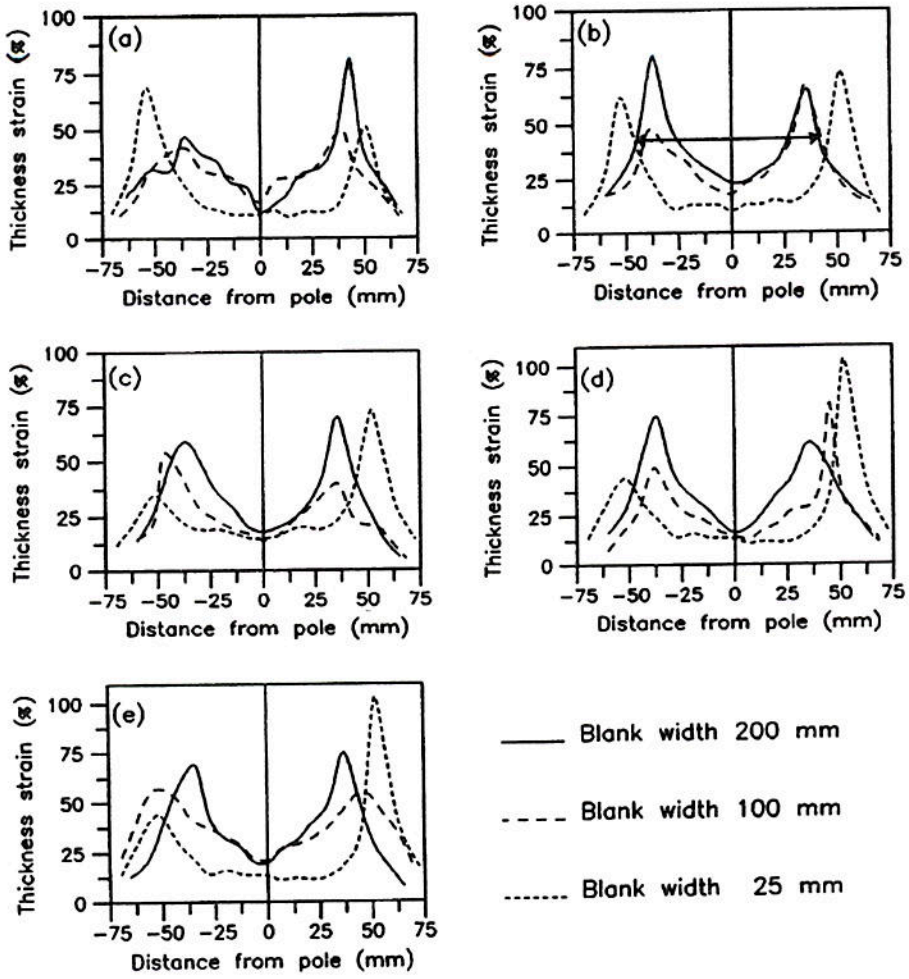

Fig. 4. Thickness strain distribution profiles in punch-stretched blanks of EDD steel for three different blank widths: (a) heat A, (b) heat B, (c) heat C, (d) heat D and (e) heat E.

deep-drawing (25 mm) than in plane strain condition. The important parameter that is used to measured the ability of the material to distribute strain is half width of thickness strain distribution (Λ), which is defined [16] as the width measured at a strain level corresponding to average of the two peak strains and it is usually called half width. This half width is geometrically determined from the strain distribution profiles as shown in Fig. 4(b).

4.6.2. Effect of n and $\bar{r}$ on strain distribution characteristics

1. First, the dependence of punch height at failure or necking on n and $\bar{r}$ was studied. Since stretchability is strongly affected by n value and drawability by $\bar{r}$ value, punch height at failure for a blank width of 200 mm, which was punch-stretched in biaxial tension was measured for all the heats and plotted against their n value in Fig. 5(a). Similarly, punch height at failure for a blank width of 25 mm, where drawing-in of the blank takes place, is plotted against $\bar{r}$ values of different heats in Fig. 5(b). The punch height increases with increase in n or $\bar{r}$ value. The correlation was reasonably good.
2. From the work of Wang and Werner [16], higher values of both n and $\bar{r}$ shift the major strain peak towards the die. So the combined effect of n and $\bar{r}$ on the distance of peak from pole was studied by measuring pole to peak distances for all the five heats for various blank widths. To avoid too much of overlapping of data points, three blank widths were selected representing three different states of strain. As shown in Fig. 6, the pole-peak distance increased with increasing $n\bar{r}$ product, for each of the blank width considered, in agreement with the result of Wang and Werner [16].
3. It was also indicated [16] that a higher n value decreases peak value of major strain while a higher $\bar{r}$ value increases $e_{1\text{peak}}$. So major strain peaks for blank widths 200, 100, and 50 mm of the five heats were plotted against the $n/\bar{r}$ values in Fig. 7. It can be seen that for plane strain condition (blank width 100 mm) and deep-drawing condition (blank width 50 mm) the $e_{1\text{peak}}$ decreases with $n/\bar{r}$ value. But in case of blank width 200 mm the

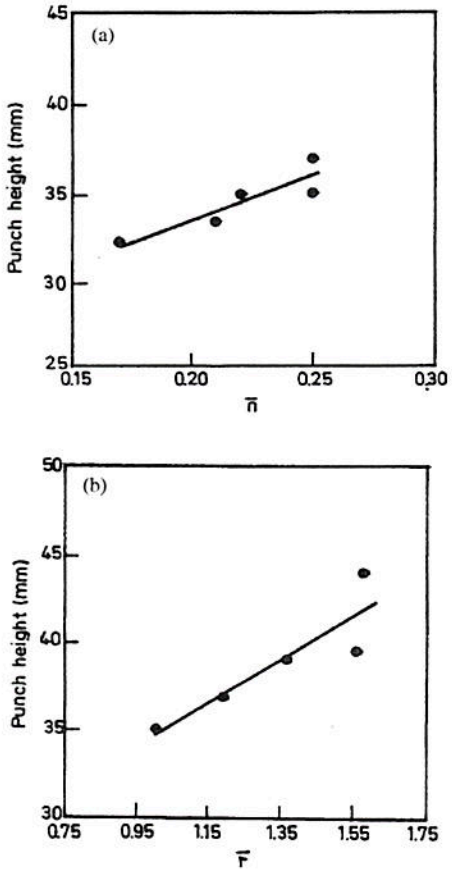

Fig. 5. (a) Effect of n value on the punch-height at failure in biaxial tension (stretching). (b) Effect of $\bar{r}$ value on the punch-height at failure in biaxial tension (deep-drawing).

correlation was poor. It may be noted that $\bar{r}$ value does not affect $e_{1\text{peak}}$ in stretching mode and due to a smaller variation of n value among the five heats (0.08), the $e_{1\text{peak}}$ for 200 mm blank remained almost constant.

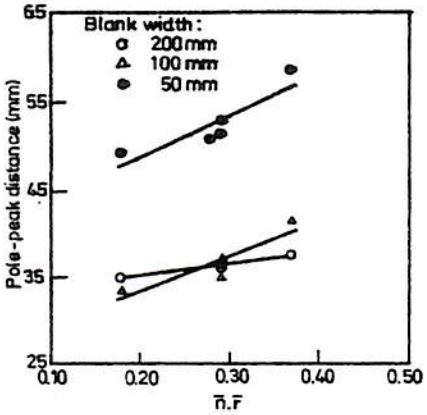

Fig. 6. Effect of product $n\bar{r}$ on pole-peak distance for three blank widths: 200 mm (biaxial tension), 100 mm (plane strain condition) and 50 mm (tension-compression).

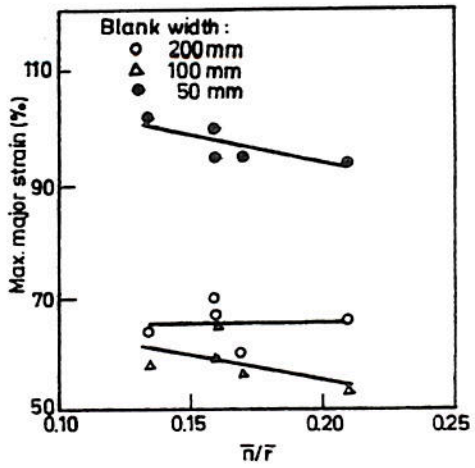

Fig. 7. Effect of $n/\bar{r}$ on the peak major strain for three blank widths: 200 mm (biaxial tension), 100 mm (plain strain condition) and 50 mm (tension-compression).

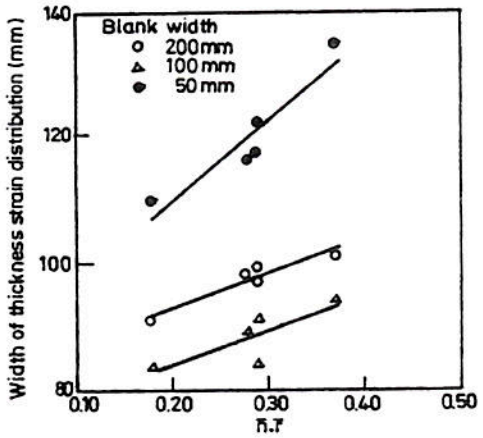

Fig. 8. Effect of the product $n\bar{r}$ on the half width of thickness strain distribution for three blank widths: 200 mm (biaxial tension), 100 mm (plain strain condition) and 50 mm (tension-compression).

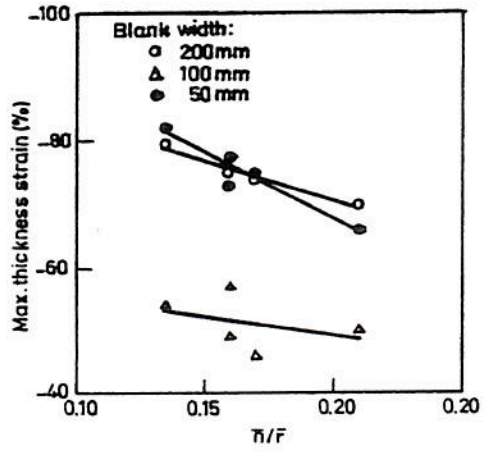

Fig. 9. Effect of the $n/\bar{r}$ on the maximum thickness strain for three blank widths: 200 mm (biaxial tension), 100 mm (plain strain condition) and 50 mm (tension-compression).

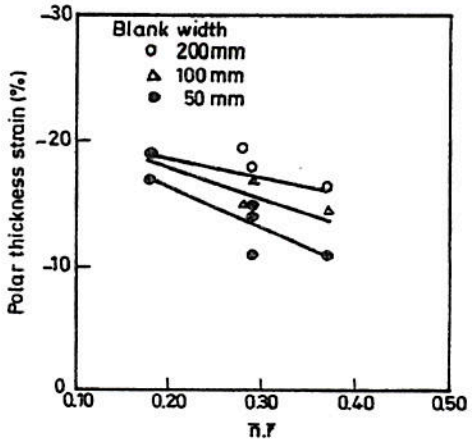

Fig. 10. Effect of the product $n\bar{r}$ on the thickness strain distribution at pole for three blank widths: 200 mm (biaxial tension), 100 mm (plain strain condition) and 50 mm (tension-compression).

4. Fig. 8 shows the variation of half width of thickness strain distribution with the product $n\bar{r}$. The linear increase of half width with the product $n\bar{r}$ is in agreement with the observations of Schedin and Melander [15] on different steels. Also, according to finite element calculations, the half width would increase with increase in both n and $\bar{r}$ values.
5. Fig. 9 shows the decrease in maximum thickness strain with $n/\bar{r}$ value. This is in agreement with finite element calculations [16] that $e_{3\max}$ decreases with decreasing values of r and with increasing values of n. But Schedin and Melander [15] concluded that $e_{3\max}$ seems to be less affected by $\bar{r}$ value than was indicated by Wang and Werner [16].
6. Finite element calculations showed that polar thickness strain is almost independent of n but increases with decreasing $\bar{r}$ value. But in the present work a satisfactory correlation was obtained between polar thickness strain and the product $n\bar{r}$ as shown in Fig. 10. It is to be noted that in all figures from 5 to 10, least squares method was used to fit the data.

5. Conclusions

Based on the results and discussions presented in the foregoing sections, the following conclusions can be drawn:

1. All the five heats contain higher carbon and manganese contents than the desired levels, which could result in lowering the formability. Only for heat D, the contents of Al and N are in the optimum range for obtaining a high $\bar{r}$ value. Except for heat A, all other heats have a favorable grain size (in range of 20–30 μm) to meet the requirements of good formability.
2. Anisotropy in mechanical properties in the sheet is only moderate. In most cases, YS and UTS values are somewhat higher at 45° to the rolling direction. Elongation to fracture is maximum in the direction of rolling. Heat B possesses higher YS and UTS values and lower ductility when compared with other heats. Heat B possesses a low n value (0.17) indicating its inferior stretchability. Other four heats have an n value in the range 0.2–0.25 and hence exhibit greater stretchability.
3. The $\bar{r}$ values of heats C and D are high and hence are suitable for critical deep-drawing applications. The heats A and B have a low $\bar{r}$ value and that of heat E is moderate. But none of the heats has an $\bar{r}$ value >1.6, which is generally expected in case of EDD grade steels. Considering overall press performance, based on the empirical index viz., the product $n\bar{r}$, heat D can be rated best followed by heats A, E, C and B in that order. Earing tendency during drawing is expected to be more for heat D due to its very high Δr value (1.02).
4. The level of the FLD increases significantly with the sheet thickness in conformity with well known earlier findings. The limit strains in the plane strain condition are lower than in the limit strains in biaxial tension and drawing for all the heats. The pattern of the FLDs in the biaxial tension zone is largely dependent on the n value and the slope of the FLDs on the left-hand side (tension-compression) is influenced by $\bar{r}$ value.
5. The strain distribution profiles reveal two major strain peaks symmetrically located about the pole. However, their magnitudes are unequal. The distance of the peaks from the pole increases with decreasing biaxiality. A study on the effect of n and $\bar{r}$ on the nature of strain distribution reveals that: (a) the punch height at failure increases with increasing n value in biaxial tension and increases with increasing $\bar{r}$ value in tension-compression, (b) the pole-peak distance increases with increasing $n\bar{r}$ product, (c) major strain peak decreases with $n/\bar{r}$ ratio, (d) the width of thickness strain distribution increases with $n\bar{r}$ product, (e) maximum thickness strain decreases with $n/\bar{r}$ value and (f) polar thickness strain decreases with $n\ \bar{r}$ value.

References

[1] G.E. Dieter, Mechanical Metallurgy, McGraw-Hill, London, 1988, pp. 295–301.
[2] Y.C. Liu, L.K. Johnson, Hill's plastic strain ratio of sheet metals, Metall. Trans. A 16 (1985) 1531–1535.
[3] W.F. Hosford, R.M. Caddell, Metal Forming-Mechanics and Metallurgy, Prentice Hall, USA, 1993, 270–308.
[4] S.S. Hecker, Simple technique for determining forming limit curves, Sheet Met. Ind. 52 (1975) 671–675.
[5] A.K. Ghosh, The effect of lateral drawing-in on stretch formability, Met. Eng. Quart. 15 (1975) 53–64.
[6] K. Swaminathan, K.A. Padmanabhan, Some investigations on the forming behavior of an indigenous extra-deep drawing low carbon steel—Part I, Trans. Indian Inst. Met. 44 (3) (1991) 231–247.
[7] N. Mizui, A. Okamoto, The effect of carbon content on the mechanical properties of continuous-annealed Al-killed sheet steels, Sumitomo Search 44 (1990) 113–119.

[8] N. Mizui, A. Okamoto, Effects of Mn content and hot band coiling temperature on deep drawability of continuous annealed Al-killed sheet steels, in: Proceedings of International Symposium on Developments in the Annealing of Sheet Steels, TMS Ferrous Metallurgy Committee, Cincinnati, OH, 1991, pp. 247–259.

[9] C. Dasarathy, R.C. Hudd, Tech. Report No. 632/A/1974, B.S.C., Strip Mill Division, Port Talbot Works, 1974.

[10] C. Dasarathy, R.C. Hudd, Tech. Rep. No. SM/PT/21/1975, B.S.C., Strip Mill Division, Port Talbot Works, 1975.

[11] R.K.P. Singh, Effect of composition and rolling parameters on the physical and metallurgical properties of EDD low carbon Al-killed steel sheets, Ph.D. Thesis, Department of Metallurgical Engineering, IIT Madras, India, 1994.

[12] D.V. Wilson, O. Acselrad, Strain localization in biaxially stretched sheets containing compact defects—I, Int. J. Mech. Sci. 26 (1984) 573–585.

[13] D.V. Wilson, A.R. Mirshams, W.T. Roberts, An experimental study of the effect of sheet thickness and grain size on limit strains in biaxial stretching, Int. J. Mech. Sci. 25 (1983) 859–870.

[14] P.B. Mellor, Sheet metal forming, Int. Metall. Rev. 1 (1981) 1–20.

[15] E. Schedin, A. Melander, On the strain distribution during punch-stretching of low and high grades of sheet steel, J. Mech. Working Technol. 15 (1987) 181.

[16] N.M. Wang, M.L. Werner, Electro-visco plastic analysis of simple stretch-forming problems, in: D.P. Koistinen, N.M. Wang (Eds.), Mechanics of Sheet Metal Forming, Plenum Press, New York, 1978, p. 367.